Structure health monitoring of composites joint reinforced by Acoustic Emission based Smart Composite Fasteners

Wenhao Li [a,b,c], Shijun Guo [a,*], Yiding Liu [d,e], Zhengquan Shen [a], Yi Xiong [c], Fei Gao [b], Darren J. Hughes [e], Jing Lin [b]

[a] *Centre of Aeronautics, School of Aerospace, Transport and Manufacturing, Cranfield University, Cranfield, MK43 0AL, UK*
[b] *Ningbo Institute of Technology, Beihang University, Ningbo, 315832, China*
[c] *School of System Design and Intelligent Manufacturing, Southern University of Science and Technology, Shenzhen, 518055, China*
[d] *School of Physics, Engineering and Computer Science, University of Hertfordshire, Hatfield, Hertfordshire, AL10 9AB, UK*
[e] *WMG, University of Warwick, CV4 7AL, UK*

ARTICLE INFO

ABSTRACT

This paper proposed an Acoustic Emission (AE) based Smart Composite Fastener (SCF) concept for health monitoring of bonded/bolted composite single lap joints. The SCF was made of 3D-printed continuous carbon fibre reinforced thermoplastic materials with an embedded piezoelectric sensor. The SCF detected signals were found to be successfully associated with AE damage sources during the loading period. It was discovered that the adhesive crack/delamination AE sources resulted in burst-type signals with identifiable onset and end, whereas AE sources of frictional sliding between the SCF and fastener holes resulted in continuous-type signals producing broad frequency content. Furthermore, the amplitudes of the burst-type signal measured from the network of SCFs were successfully correlated with the locations of the damages. In the direction away from the damage, the amplitudes of the burst-type voltages measured from the SCF showed a decreasing trend, with 10195mv, 9,995mv, and 7,426mv respectively. Generally, the research in this paper explores the correlation between the voltage signal from a damaged AE source and the SCF, providing the feasibility of using a novel SCF for health monitoring in composite joint structures.

1. Introduction

Composite materials are widely used in aircraft primary structures owing to their superior strength properties over metallic materials. However, due to the variations and discontinuities in the geometries of aircraft structures, the composite structures have to be bonded to form the major components, and the structural bonding quality is affected by many factors which can often be a critical threat to structural integrity and efficiency [1–3]. The primary bonded structure failures would generally result in a catastrophic loss of the aircraft. Consequently, the large and heavy aircraft structures need to be monitored on a regular basis to detect the defects and determine the remaining life.

Structural health monitoring (SHM) is broadly applied in engineering structures, allowing for condition-based maintenance to reduce repairing costs and improve structural safety margin set [4–6]. Damage caused by mechanical injury, environment change, or aging of mechanical structure results in strain change abruptly. Piezoelectric sensors, one of the most commonly used materials for SHM, can be used for actuating under electric field and sensing the reaction, owing to their electro-mechanical coupling effect [7]. Due to its high sensitivity, high signal-to-noise ratio, and rapid reaction time, small and conformal piezoelectric sensors are well-suited for the determination of pressure, acceleration, strain, force, and high-speed impact load measurements [8]. They are being widely either surface mounted or embedded into the structures for continually monitoring the target structure. Some research efforts have developed structure health monitoring for the bolted SLJs. Doyle et al. investigated the acoustic-elastic and electro-mechanical impedance methods based on self-diagnostic techniques for detecting the loosened bolts by assembling an active piezoelectric wafer sensor network [9]. The technology has shown the capability to detect and locate loosened bolts in a reasonable range. Similarly, Demetgul et al. evaluated the condition of the riveted joints based on an active and passive method. The active method used leadzirconate titanate (PZT) to generate Lamb waves and monitor their propagation, and the passive

method used Fibre Bragg Grating sensors to evaluate the spectral characteristic of the signals based on Fast Fourier Transformation [10]. The results indicated that using both approaches together can estimate the missing rivet's locations and evaluate the health condition of the joints.

However, one of the challenging issues of using surface-mounted sensor is that it changes the wing shape and affects aerodynamic load transfer [11]. One of the solutions is to embed sensors into the host structures. Nevertheless, the monitored structure embedded with sensors can be considered a typical model containing inclusion due to the different material characteristics between the host material and the PZT sensor, and the contact interface is prone to debonding failure under high interfacial shear load [12]. Attempts have been made to address this issue. Wang et al. proposed a new concept of smart composite joints, integrating eddy current sensor foils and piezoelectric sensors into the fasteners to develop smart composite joints with multifunctional sensing capabilities, which can autonomously sense the external environment events and the fastener connection status [13]. The above studies have mainly focused on mechanical bolted joints. The combination of mechanical bolted and bonded joints has been widely employed to safeguard aircraft structures. Compared to the bolted joint, they have more complex failure modes due to the structural non-linear behavior and uneven distribution characteristics of load transfer [14,15], however, limited research has been carried out in this field.

Acoustic Emission (AE) monitoring is a passive and dynamic monitoring method that detects energy from the monitored object itself, not dependent on other power sources, and is a popular technology currently applied to the health monitoring of composite joint structures [16]. In this study, a new concept of AE-based Smart Composite Fastener is proposed as an alternative to the traditional SHM method, which can meet the demand for fast response and low energy consumption SHM without compromising the aerodynamic performance and structural reliability of the composite aircraft structures. The research is carried out in a more qualitative approach and a few key features are accomplished: 1) The failure mode was found to be related to output signal types. Adhesive crack/delamination generates a burst-type signal, while the SCF loosen generates a continuous-type signal. 2) In networks formed by SCFs, the amplitude of the burst-type signal varies with the location of the damage.

2. Experiment

The Single-Lap Joints (SLJs) of $200 \times 20 \times 3.6$ mm^3 were manufactured of woven CFRP laminates, which consisted of 12 plies sheets in 0/90 orientation. The overlap region was bonded using Redux420® adhesive. Three holes of 8 mm diameter were drilled along the center line of the overlap region at 20 mm intervals to reinforced by Smart Composite Fasteners (SCFs). The detailed dimensions of the SLJs reinforced by SCFs are shown in Fig. 1(a). To fabricate the SCFs, the composite fasteners were firstly manufactured by a 3D printing machine Mark Two desktop, followed by the assembly of piezoelectric sensor. The 3D-printed composite fasteners consisted of two filament feedstocks, one is continuous carbon fibre filament and the other one is Onyx (matrix) filament, as described in Ref. [2]. As shown in Fig. 1(b), the composite fasteners were manufactured with a length of 14 mm and diameters of 8 mm and 14 mm for the head and body respectively. A through-out hole of 3 mm diameter was made in the center of the base composite fastener to accommodate a piezoelectric sensor inserted into the hole. The sensor was fixed with composite fastener through filled epoxy to form the SCFs. The piezoelectric sensor of P5 type was obtained from Nippon Electric Company, Ltd. (Japan) with a dimension of $5 \times 1.65 \times 1.65$ mm^3. The properties of the P5 PZT sensor are summarized in Table 1 provided by the manufacturer.

After assembly of the SCFs into the SLJs, the Distributed Optical Fibre Sensor (DOFS) provided by Luna Ltd was installed on the laminate

Table 1
Parameters of the P5 PZT sensor.

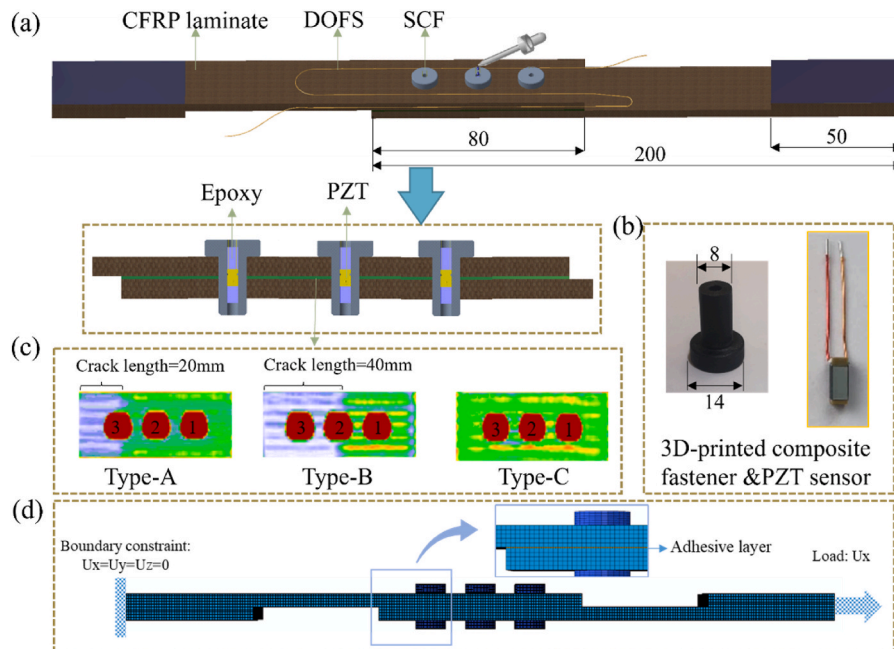| Parameters	Values
Piezoelectric Charge constant, d_{33} (C/N $\times$ 10^{-12})	460
Piezoelectric Voltage constant, g_{33} (10^{-3} Vm/N)	27
Resonant frequency, f (kHz)	40
Relative Dielectric constant, K_{33}^T	2800
Transverse coupling co-efficient, K_{31}	0.37
Longitudinal coupling co-efficient, K_{33}	0.72
Coupling coefficient, K_p	0.63
Measured Capacitance, C (nF)	3.28
Measured impedance, I (Ω)	170

Fig. 1. (a) Dimension of the SLJ and configuration of the SCF (unit in mm), (b) 3D-printed composite fastener and piezoelectric sensor, (c) C-scan results of the SLJs with different bonding conditions. (d) FE model of the SLJ reinforced by SCFs.

surface over the overlap area by using adhesive tape, as shown in Fig. 1 (a). Herein we examine Rayleigh scattering based optical fibre sensors due to their high chemical stability and small diameters. When an electromagnetic wave is launched into an optical fibre, the light will be redistributed by Rayleigh scattering [17]. If the local changes in temperature and strain are relayed to the optical fibres, the scattered signal in the fibre will be modulated by these physical parameters. Coherent Optical Frequency Domain Reflectometry (C-OFDR), a type of Rayleigh scattering based DOFS, is performed to monitor distributed strain and temperature of the anode electrode, due to its high spatial resolution (2.6 mm) measurement capability. To leave enough space for the DOFS installation, the blank tail-end SCFs were directly used for assembling. The blank tail-end was glued with laminate hole using Redux420® adhesive, to prevent the pull-out of SCFs during the test. The SLJs samples prepared in this study were designed with different debonding lengths in the overlap region. Fig. 1(c) shows the ultrasonic C-scan results of SLJs with debonding of 0 mm to 40 mm seeded from the overlap edge close to the SCF 3.

A numerical model was built to simulate the stress distribution in the SLJ reinforced by SCFs using ABAQUS®/Explicit software, to compare and validate the results obtained from DOFS. The FE mesh and boundary conditions set for the SLJ reinforced by SCFs are shown in Fig. 1(c). The adherends, fasteners and adhesive layer were modelled with three-dimensional solid element C3D8R. The contact surface between the SCFs and two adherents was defined by the surface-to-surface algorithm. The material data for MTM46/HTS and adhesive Redux420® were found in Ref. [1]. The material properties of the 3D-printed composite materials used in this study were taken from Ref. [2], where the same filament material and manufacturing process were used.

Fig. 2 shows the experiment test set-up for the SLJs including the piezoelectric sensor and optical fibre sensor measurement system. The SLJs were tested at a loading rate of 1 mm/min until failure by displacement control, using an INSTRON machine equipped with a 50 kN load cell. The piezoelectric sensor measurement system consisted of a charge amplifier and a data acquisition system, connecting through wires, with a data acquisition rate of 20Hz. The DOFS was connected to ODiSI-B system with a data acquisition rate of 20Hz.

3. Results and discussion

The test results of type-A, B and C bonded SLJs reinforced by SCFs are shown in Figs. 3–5 respectively. Each Figure (a) shows the load against displacement curves of the SLJs. The corresponded voltage outputs from SCF 1, 2, and 3 measured by the piezoelectric sensor system are plotted in Figure (b). As shown in Fig. 3/4/5 (a) and (b), as the load applied increased linearly, the voltage measured from the SCFs remained at zero. The voltage signals measured from SCFs were not varied with the increase of the load applied to the SLJs. This is due to loading frequency is reltively low and the piezoelectric sensor will not respond to the load at low frequency [18].

However, when the applied load gradually increased to a higher level, voltage signal was detected, accompanied by the noise generated from the onsite damage of the specimens. To relate the voltage signal with the structure damage, tests were then suspended followed by on-site damage observation using the traveling microscope, as shown in Figure (c). Longitudinal strains (ε_{11}) measured by DOFS along the attached path at different periods are plotted in Figure (d), together with the FE model simulated results for validation and comparison.

3.1. Type-A SLJ

The first burst-type signal of type-A SLJ occurred when the load reaches 18.3 kN at 79.1 s, marked as point (I) in Fig. 3(a). The amplitude of voltage signal measured from SCF 1 was 8051 mv, however, SCF 2 and 3 had no apparent burst-type signal. In Fig. 3 (c), traveling microscope observation at point (I) showed delamination propagating in the adherends nearing the overlap edge (green triangle side), with the adhesive bonding remaining bonded. In Fig. 3 (d), before the damage occurred (point I), the measured strain in blued triangle side had a more rapid growth trend. Subsequently, after the damage occurred (point I), strain in the green triangle side decreased, and the strain in the blue triangle path started to rapid growth and surpass the green triangle path. This suggested that the green triangle path side dominated the load transfer resulting in the delamination damage, which can further explain the experimental observation.

The second set of signals were detected from 82 s until failure of the joint, in addition to the burst type signal at the final failure point, it also contained the continuous-type signal. Different from burst-type signals with identifiable beginning and end, typically on a timescale between *μs and ms*, the continuous-type source produced a broad range of frequency content. Further observation in Fig. 3(c)-II showed that the SLJ fractured with interface debonding, along with the SCF pull-out and shear mode failure. This finding suggested that there is a strong correlation between the SCF voltage signal and the damage type. Washabaugh and Knauss [19] reported that Mode-I crack propagation over a weak interface can approach the material's Rayleigh wave speed (C_R), which is faster than a crack propagating in a bulk medium that can only reach half of the C_R due to crack branching. Under mode-II loading, Rosakis et al. [20] found that the interface bonding crack propagation speed exceeds the shear wave speed of the material (C_S) and becomes intersonic. On-site of the micro- or macro-crack failure, elastic stress waves were generated by the sudden release of stored elastic energy at a very fast speed, resulting in the generation of burst-type signals. Thereafter, with the increase of the applied load, the shear load and out-of-plane bending led to the friction sliding between the SCF and laminate hole, resulting in the generation of continuous-type AE signals.

3.2. Type-B SLJ

The first burst-type signal of type-B SLJ occurred when the load reaches 16.9 kN at 75.6 s, marked as point (I) in Fig. 4(a). Similarly, the burst-type signal of 6958 mV amplitude at 75.6 s was only detected by
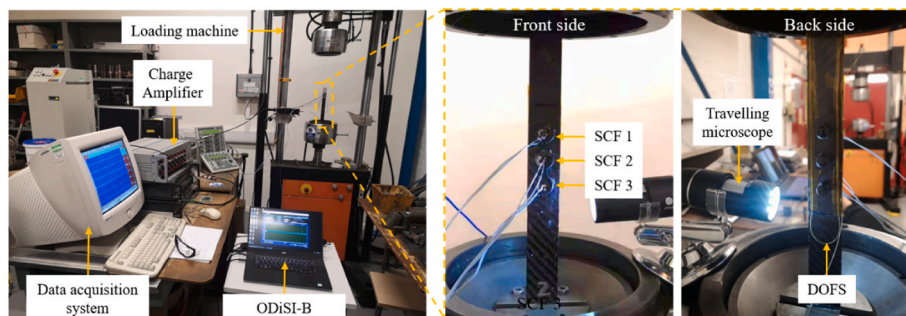

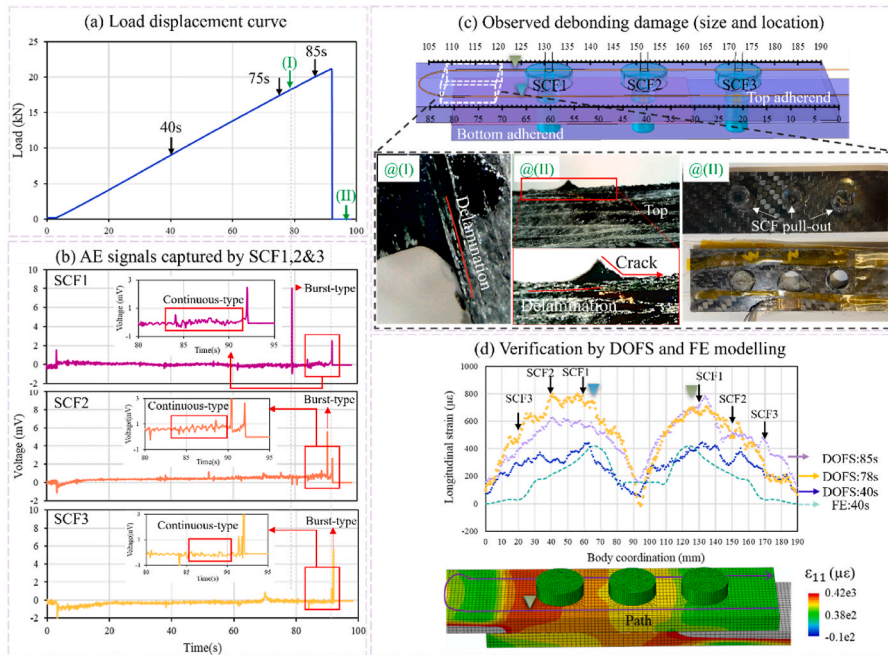**Fig. 2.** Experiment set-up including the SCF and DOFS measurement systems.

Fig. 3. Experiment and FE modelling results of type-A SLJ: (a) The load-displacement curve of the measured SLJ sample; (b) The AE signals captured by SCF 1,2 and 3; (c) The observations of sizes and locations of the debonding damages in the joint associated with the sample images; (d) The comparison of longitudinal strains measured from DOFS and FE modelling corresponded to the DOFS path.

Fig. 4. Experiment and FE modelling results of type-B SLJ: (a) The load-displacement curve of the measured SLJ sample; (b) The AE signals captured by SCF 1,2 and 3; (c) The observations of sizes and locations of the debonding damages in the joint associated with the sample images; (d) The comparison of longitudinal strains measured from DOFS and FE modelling corresponded to the DOFS path.
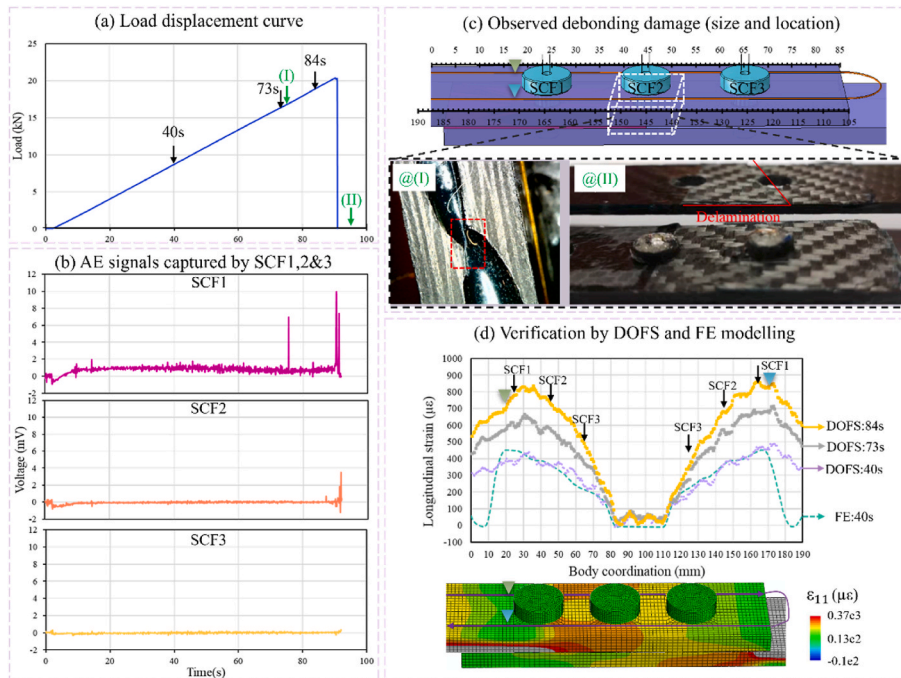
SCF 1, as shown in Fig. 4(b). Inspection at point (I) found that the wire had lost its connection to SCF 3. The voltage signal from SCF1 and SCF 2 were used for the following discussion. Observation under the traveling microscope in Fig. 4(c)@(I) showed that delamination propagation initiated near the SCF 2. The SLJs joints finally failed in delamination with adhesive debonding, along with the SCF pull-out and shear mode failure, as shown in Fig. 4(c)@II. Fig. 4 (d) revealed that the strain

measured between two loading paths showed similar values and variation trends before and after point (I).

It should be noted that the voltage signal at the same time detected by SCFs in the network had different magnitudes or modes. Several factors could explain this: Firstly, regarding the directional nature of the damage and predominant mode, different AE sources can generate two types of AE mode: in the plane of the plate (IP) for the extensional mode
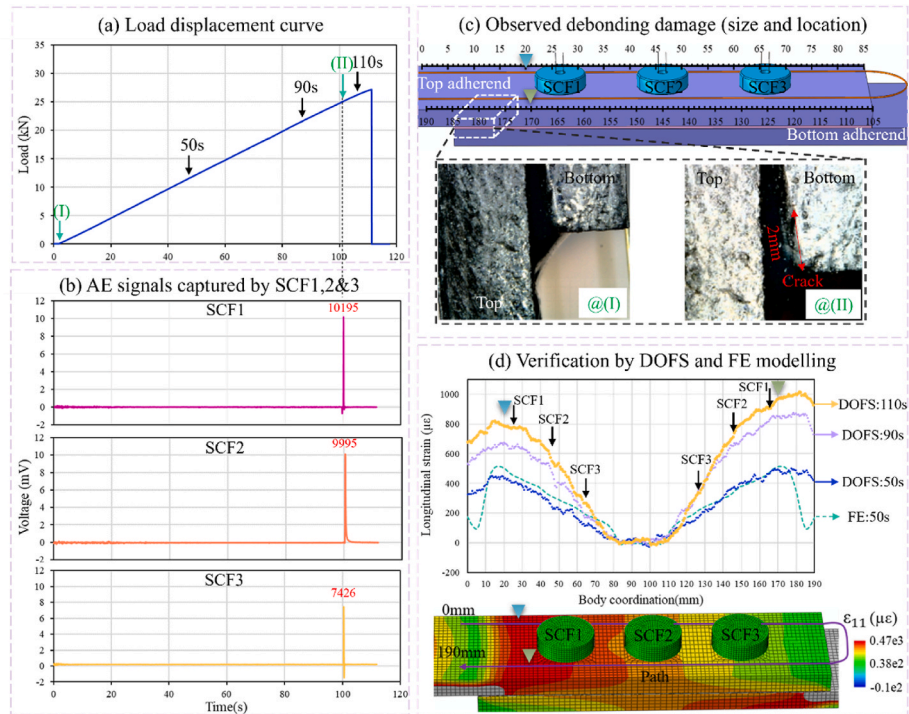
Fig. 5. Experiment and FE modelling results of type-C SLJ: (a) The load-displacement curve of the measured SLJ sample; (b) The AE signals captured by SCF 1,2 and 3; (c) The observations of sizes and locations of the debonding damages in the joint associated with the sample images; (d) The comparison of longitudinal strains measured from DOFS and FE modelling corresponded to the DOFS path.

and outside to the plane of the plate (OP) for the flexural mode. In this regard, depending on the predominant mode, even sensors in the same positioning array often do not receive stress waves in the same mode [21]. Secondly, due to the multi-layered geometry and non-homogeneous nature of the bonded/bolted joint properties, AE wave propagation in the structure with various attenuation trends [22]. Thirdly, the piezoelectric sensor sensing mechanism is also directional-dependent, only when the stress wave arrived at specific directions, such as d_{33} and d_{15}, could maximum the voltage output.

3.3. Type-C SLJ

The burst-type signal of type-B SLJ occurred when the load reached 25.7 kN at 100.1 s, marked as point (II) in Fig. 5(a). By comparing the picture taken at the beginning point (I) and point (II), verified the occurrence of crack propagation, initiated from the adhesive edge close to SCF1 with a length of 2 mm, as shown in Fig. 5(c). The amplitudes of burst-type voltages measured from SCF 1, 2, and 3 were 10195 mv, 9995 mv, and 7426 mv, respectively with a decreasing tendency. This attenuation tendency indicated that the AE source generated elastic stress wave propagated from SCF1 to SCF3, which was agreed with the observed damage location. Longitudinal strain (ε_{11}) measured by DOFS along the whole attached path at 50 s, 90 s, and 110 s were plotted in Fig. 5(d). At 50 s, symmetrical paths located on both side of the SCFs showed a similar strain variation trend with the increase of load, which were verified by the FE simulation. However, as the load increased further, the path marked by the green triangles showed a more rapid growth trend than the blue triangle path till the final failure. The stress distribution over the laminate surface indicated that the load transfer on the symmetrical path is not identical. The uneven distribution of the adhesive could explain the difference, as the load transfer varies with the thickness of the adhesive layer. The thinner the thickness of adhesive, the higher the load transfer and stress level [23]. The strain distribution across the overlap agreed well with the experiment observation, which was consistent with the data obtained from the voltage signal of SCF.

The SCF of type C SLJ failed to detect any voltage signal after the first set of signals were detected. Compared to type A and B SLJs, the first burst type signal detected in type C SLJ at a higher load level with higher voltage amplitude indicates that a large amount of stored energy was released on site of the crack. This could result in the adhesion loss and interface cracking between the sensor and composite fastener, leading to the discontinuity in the stress waves propagation [24].

4. Conclusion and future work

A concept was developed for structure health monitoring (SHM) by using a novel Acoustic Emission (AE) based smart composite fastener (SCFs) that can be mounted in a structure joint for reinforcement. The feasibility and application potential of this method is demonstrated by experiment and numerical simulation of composite SLJs as an example. The results of this study show that the burst-type and continuous-type output voltage from SCFs is correlated with the different types of AE sources in response to different damage types occurred, verified by observations under the traveling microscope and measured strain using Distributed optical fibre sensors (DOFS). Also, the magnitude of the voltage signals measured by SCFs determined by a variety of factors was clarified, such as the directional fracture behavior of the AE source, and the multilayer and non-homogeneous nature of the composite joining structure, and the orientation-dependent electro-mechanical properties of the piezoelectric sensor. This study has provided a new strategy for structure health monitoring of composite SLJ by using the AE source-based Smart Composite Fasteners. Future research will carry out the modal analysis to separate the modes of different source AE waves, making it possible to extract information about the source event in a more quantitative method.

CRediT authorship contribution statement

Wenhao Li: Formal analysis, Data curation, Software, Writing – original draft, Writing – review & editing. **Shijun Guo:**

Conceptualization, Methodology, Validation, Funding acquisition, Resources, Writing – review & editing, Supervision. **Yiding Liu:** Experiment, Validation, Writing – review & editing. **Zhengquan Shen:** Experiment. **Yi Xiong:** Experiment, Validation. **Fei Gao:** Writing – review & editing. **Darren J. Hughes:** Resources. **Jing Lin:** Writing – review & editing, Resources.

Declaration of competing interest

The authors declare that they have no known competing financial interests or personal relationships that could have appeared to influence the work reported in this paper.

Acknowledgments

References

[1] W. Li, S. Guo, I.K. Giannopoulos, S. He, Y. Liu, Strength enhancement of bonded composite laminate joints reinforced by composite Pins, Compos. Struct. 236 (2020), 111916.

[2] W. Li, S. Guo, I.K. Giannopoulos, M. Lin, Y. Xiong, Y. Liu, Z. Shen, 3D-printed thermoplastic composite fasteners for single lap joint reinforcement, Compos. Struct. 282 (2022), 115085.

[3] Y. Wan, W. Hu, B. Yang, X. Zhao, G. Xian, Y. Yuan, L. He, C. Liu, J. Deng, On-line tensile damage monitoring of WGF/epoxy T-joint by the embedded MWCNT@ WGF sensor, Compos. Commun. 23 (2021), 100541.

[4] L. Yuan, W. Fan, X. Yang, S. Ge, C. Xia, S.Y. Foong, R.K. Liew, S. Wang, Q. Van Le, S.S. Lam, Piezoelectric PAN/BaTiO3 nanofiber membranes sensor for structural health monitoring of real-time damage detection in composite, Compos. Commun. 25 (2021), 100680.

[5] N. Forintos, T. Sarkadi, T. Czigany, Electric resistance measurement–based structural health monitoring with multifunctional carbon fibers: predicting, sensing, and measuring overload, Compos. Commun. 28 (2021), 100913.

[6] M. Lin, S. Guo, S. He, W. Li, D. Yang, Structure health monitoring of a composite wing based on flight load and strain data using deep learning method, Compos. Struct. 286 (2022), 115305.

[7] V.T. Rathod, A review of electric impedance matching techniques for piezoelectric sensors, actuators and transducers, Electronics 8 (2) (2019) 169.

[8] V.T. Rathod, A review of acoustic impedance matching techniques for piezoelectric sensors and transducers, Sensors 20 (14) (2020) 4051.

[9] D. Doyle, A. Zagrai, B. Arritt, Bolted joint integrity structural health monitoring for responsive space satellites, in: 50th AIAA/ASME/ASCE/AHS/ASC Structures, Structural Dynamics, and Materials Conference 17th AIAA/ASME/AHS Adaptive Structures Conference 11th AIAA No, 2009, p. 2705).

[10] M. Demetgul, V.Y. Senyurek, R. Uyandik, I.N. Tansel, O. Yazicioglu, Evaluation of the health of riveted joints with active and passive structural health monitoring techniques, Measurement 69 (2015) 42–51.

[11] Z. Ma, X. Chen, Fiber Bragg gratings sensors for aircraft wing shape measurement: recent applications and technical analysis, Sensors 19 (1) (2018) 55.

[12] H. Wang, L. Jiang, P. Xiang, Improving the durability of the optical fiber sensor based on strain transfer analysis, Opt. Fiber Technol. 42 (2018) 97–104.

[13] Y. Wang, X. Qing, L. Dong, S. Banerjee, Multi-field coupled sensing network for health monitoring of composite bolted joint, in: Health Monitoring of Structural and Biological Systems 2016 vol. 9805, International Society for Optics and Photonics, 2016, April, p. 98052L.

[14] S. Guo, W. Li, Numerical analysis and experiment of sandwich T-joint structure reinforced by composite fasteners, Compos. B Eng. 199 (2020), 108288.

[15] Y. Liu, C. Carnegie, H. Ascroft, W. Li, X. Han, H. Guo, D.J. Hughes, Investigation of adhesive joining strategies for the application of a multi-material light rail vehicle, Materials 14 (22) (2021) 6991.

[16] S. Teixeira de Freitas, D. Zarouchas, J.A. Poulis, The use of acoustic emission and composite peel tests to detect weak adhesion in composite structures, J. Adhes. 94 (9) (2018) 743–766.

[17] B. Lee, Review of the present status of optical fiber sensors, Opt. Fiber Technol. 9 (2003) 57–79, https://doi.org/10.1016/S1068-5200(02)00527-8.

[18] J. Liu, X. Luo, J. Liu, M. Li, L. Qin, Development of a commercially viable piezoelectric force sensor system for static force measurement, Meas. Sci. Technol. 28 (9) (2017), 95103.

[19] P.D. Washabaugh, W.G. Knauss, A Reconciliation of Dynamic Crack Velocity and Rayleigh Wave Speed in Isotropic Brittle Solids, Kluwer Academic Publishers, 1994.

[20] A.J. Rosakis, O. Samudrala, D. Coker, Cracks Faster than the Shear Wave Speed, 1964 [Online].

[21] M. Surgeon, M. Wevers, Modal analysis of acoustic emission signals from CFRP laminates, NDT E Int. 32 (6) (1999) 311–322.

[22] F. Dahmene, S. Yaacoubi, M. El Mountassir, N. Bendaoud, C. Langlois, O. Bardoux, On the modal acoustic emission testing of composite structure, Compos. Struct. 140 (2016) 446–452.

[23] M.D. Banea, L.F.M. da Silva, R.D. Campilho, The effect of adhesive thickness on the mechanical behavior of a structural polyurethane adhesive, J. Adhes. 91 (5) (2015) 331–346.

[24] S.A. Haddadi, A. Ramazani Sa, M. Mahdavian, P. Taheri, J.M.C. Mol, Mechanical and corrosion protection properties of a smart composite epoxy coating with dual-encapsulated epoxy/polyamine in carbon nanospheres, Ind. Eng. Chem. Res. 58 (8) (2019) 3033–3046.